Academic Journal of Science and Technology
ISSN: 2771-3032 | Vol. 20, No. 3, 2026

Comparison of Performance and Life of Threaded Holes under Different Forming Processes

Jiaheng Pi

School of Mechanical Engineering, Xi'an Shiyou University, Xi'an, Shaanxi 710065, China

Abstract: This paper systematically compares the differences in microstructure, mechanical properties, and fatigue life of non-magnetic drill collar threaded holes fabricated by two forming processes: cold extrusion and machining. The research primarily involved material characterization through microscopic observation, hardness testing, and mechanical property analysis. Fatigue tests were conducted to obtain life data under various stress levels and to construct S-N curves, with particular attention to the inflection points and fatigue limits. High-frequency three-point bending fatigue tests were performed on full-scale bolt specimens produced by both machining and cold extrusion, under a stress ratio of R=0.1 and frequencies ranging from 10 to 30 Hz. The tests employed rectangular cross-section specimens with a span of 160 mm, subjected to sinusoidal wave loading using an Instron electro-hydraulic testing machine, while crack initiation at the threaded holes was closely monitored. Based on the experimental data, the fatigue life, scatter, and allowable design stress of the two processes were compared. The experimental parameters included thread forming method (cold extrusion/machining), microhardness, surface roughness, and tensile strength. The results indicate that the fatigue performance of the cold extrusion process is significantly superior to that of the machining process. At a stress amplitude σ_a= 345.6 MPa, the fatigue life of the extruded specimens was approximately 4.1 times that of the machined specimens, with a notably lower scatter band factor (1.42 vs. 8.69), indicating superior performance stability. Fitting using the Basquin equation yielded a fatigue strength coefficient σ'_f = 1132.6 MPa and exponent b = -0.1097 for the machining process, compared to σ'_f = 3033 MPa and b =-0.1777 for the extrusion process. At a design life of 10^5 cycles, the allowable stress amplitudes for the machined and extruded threads were 270 MPa and 300 MPa, respectively, corresponding to actual safety factors of 1.28 and 1.15. This suggests that fatigue failure in these cases is dominated by local plastic strain. The extrusion process effectively reduces the fatigue notch factor by introducing surface compressive residual stress and improving the material state around the notch, thereby extending fatigue life. In summary, the cold extrusion process offers significant advantages in high-cycle fatigue applications. It is therefore recommended for use in the design of critical load-bearing components, and that stress concentration effects and process-induced performance variations be fully accounted for in fatigue life assessment to enhance structural reliability and service life.

Keywords: Non-Magnetic Drill Collar; Cold Extrusion And Cutting; Mechanical Properties; Fatigue Properties; S-N Curve; Allowable Stress Amplitude.

1. Introduction

As a key component in oil and gas drilling and production, the non-magnetic drill collar not only provides sufficient drilling pressure for the bit but also significantly enhances the stiffness of the drill string. In addition, it offers a non-magnetic environment for magnetic measurement instruments, ensuring the accuracy of measurement data and the vertical precision required in deep drilling operations[1]. Over the past decade, with continuous advancements in oilfield exploration, development, and drilling technologies, logging-while-drilling (LWD) systems have been increasingly applied in directional drilling operations. As drilling depth and difficulty increase substantially, higher safety requirements are imposed on downhole tools. Since the attitude measurement module in LWD systems must operate in a non-magnetic environment, the drill collar is typically made of high-nitrogen austenitic stainless steel, which possesses excellent mechanical properties, good corrosion resistance, and extremely low magnetic permeability, making it the preferred material for non-magnetic drill collars[2].

Nitrogen and manganese are introduced into austenitic stainless steel as stabilizing elements to partially replace the more expensive nickel, thereby significantly reducing material costs. In addition, nitrogen alloying enhances resistance to localized corrosion and improves corrosion performance in certain environments. Consequently, high-nitrogen austenitic stainless steel is a structural material with good mechanical properties, excellent corrosion resistance, and broad application prospects. However, the thin-walled structures that result from machining are prone to excessive stress and even crack defects when subjected to complex loads such as axial force, bending, torsion, and impact, which can reduce the service life of non-magnetic drill collars. Currently, the materials commonly used for drill collars worldwide are Cr-Mn series high-nitrogen austenitic stainless steels, with typical grades including P550 and P650 from Austria, and 15-15 and 15-15HS Max from the United States. These materials exhibit a stable single-phase austenitic structure and reliable non-magnetic properties[3].

This study focuses on two cracks observed at the edge of an M8 internal threaded hole located at the corner of the cover slot at the bottom of a failed LWD instrument drill collar. The structural configuration of the instrument drill collar and the crack in the M8 threaded hole within the cover slot are shown in Figure 1. The material used is imported P550 high-nitrogen austenitic stainless steel[4]. This non-magnetic drill collar had a cumulative service time of 526 hours and a total footage of 10,000 meters, with the maximum bending moment generated under a dogleg severity of 18°/30 m accounting for 2% of downhole operating conditions. The threaded holes of this drill collar were still manufactured using the traditional

cutting process. Cold extrusion of internal threads offers advantages such as improved surface quality, higher strength, and better fatigue resistance. In contrast to cutting, which often introduces defects such as cutting heat, burrs, and microcracks due to tool friction, cold extrusion achieves uniform deformation under high pressure, resulting in a more even distribution of internal stress and fewer structural defects, thereby enhancing both tensile strength and fatigue performance. This technology has been applied in fields such as aerospace, petroleum drilling, and ship transportation. However, research on the cold extrusion process for internal threads in China still lags behind that in developed countries, with progress being relatively slow[5].

Figure 1. Crack initiation source and propagation direction of the threaded hole in the non-magnetic drill collar

2. Material Inspection Plan

The chemical composition of the non-magnetic drill collar material is shown in Table 1. The cracked portion of the threaded hole at the bottom of the cover slot was separated from the drill collar using wire electrical discharge machining. The crack was then opened to expose the threaded fracture surface, and the morphology was observed under a Zeiss scanning electron microscope. A block-shaped specimen measuring 10mm × 10mm × 30mm was cut from the drill collar near the crack. The specimen was sequentially ground with water abrasive paper from 100 to 1200 grit, mechanically polished, and then etched with an etching solution (a mixture of 5g $CuCl_2$, 25mL hydrochloric acid, and 25mL alcohol). Metallographic structure was observed using an Observer A1m optical microscope, and hardness was measured using a hardness tester. Specimens were taken from the thick-walled section of the drill collar to prepare rod-shaped tensile specimens with dimensions of φ12.5mm × 50mm and V-notched impact specimens with dimensions of 10mm × 10mm × 50mm. Tensile and room-temperature impact tests were conducted using a Z600 universal material testing machine and a pendulum impact tester, respectively.

Table 1. Chemical composition of the non-magnetic drill collar material (wt%)

element	C	Si	Mn	P	S
P550	0.0353	0.402	17.88	0.0174	0.0248
element	Cr	Mo	Ni	N	Fe
P550	19.30	1.68	4.07	0.62	The rest

In this study, two 100mm long strip specimens were selected, and four M8 internal threaded holes were machined in each using cutting and cold extrusion processes, respectively. Each threaded hole was sectioned along the centerline by wire electrical discharge machining. The cross-sections were sequentially ground and polished, and microhardness was measured using a Vickers hardness tester at five points spaced at 120μm intervals from the thread root and flank toward the base material. The microstructure of the specimens was revealed using an etchant. Referring to the actual structure of the drill collar, six simulated test specimens with dimensions of 400mm × 30mm × 25mm were prepared. A small cover slot and two M8 threaded holes were machined in the middle of each specimen, with three specimens processed by cutting and three by cold extrusion, as shown in Figure 2. During the test, the cover plate was installed, and A4-80 grade M8×1.25 screws were tightened with a torque of 30N·m. High-frequency three-point bending fatigue tests were conducted on an Instron electro-hydraulic servo fatigue testing machine. The test setup included a span of 160mm, with a sinusoidal wave at 10Hz, a stress ratio of 0.1, and a maximum stress of 60kN, simulating the bending condition of the drill collar under a maximum dogleg severity of 18°/30 m. The specimens were disassembled every half hour to carefully inspect crack development in the threaded holes, and the test was terminated when obvious cracks appeared. Subsequently, the threaded hole cracks were sectioned, and the fracture source morphology was observed using a Keyence VHX-7000N ultra-depth-of-field microscope. The initiation location of the fatigue source was examined to analyze the fatigue failure mechanism.

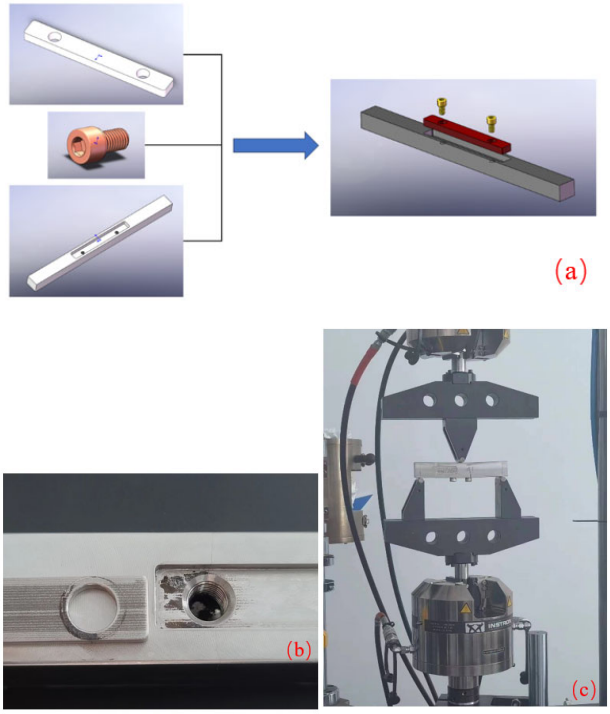

(a)Assembly drawing of the simulated part;(b)Cracks appear at the edge of the threaded hole under the cover plate;(c)Three-point bending fatigue test

Figure 2. Three-point bending fatigue test of the simulated drill collar specimen

3. Experimental Results

3.1. Macroscopic and microscopic morphology of the threaded hole of the failed part

The morphologies of the cut thread and the cold extruded thread under the microscope are shown in Figure 3 and Figure 4.

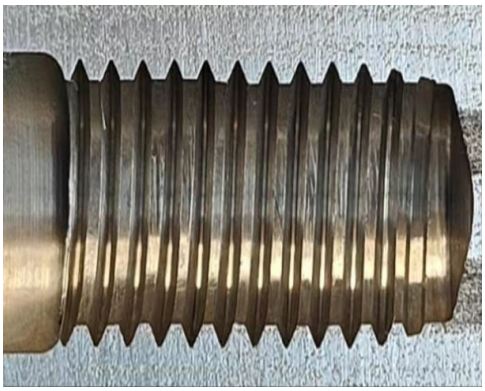

Figure 3. Cut thread

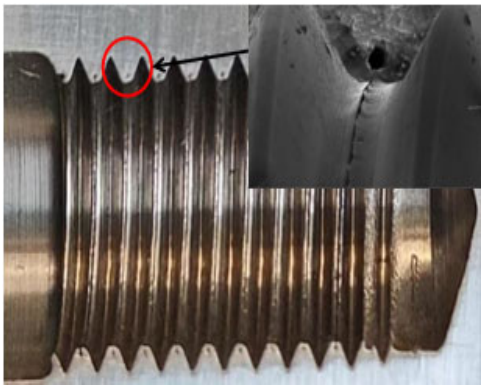

Figure 4. Rolled thread

Bolt hole processing is often applied to the cover plate groove of drill collars, and most of such failures are caused by cracking of the bolt hole in the cover plate groove. To reduce such failure incidents, the performance of bolt holes produced by two different processing techniques was tested and compared, the differences in thread performance between the extrusion (rolled) and cutting (machined) processes were analyzed, and the optimal, most suitable bolt hole processing technique was selected. The basic principle of cold extrusion is to utilize the plastic deformation characteristics of materials at low temperatures. During the deformation process, the crystal structure inside the metal changes, typically resulting in a cold work hardening effect, thereby increasing the strength and hardness of the material. The thread morphologies of the two processing techniques were observed under a scanning electron microscope. For the extruded thread, plastic deformation occurs on the surface of the extruded material, with both sides stacking toward the center to form a groove-like structure, as shown in Figure 5. The surface of the cut thread is relatively smooth, as shown in Figure 6.

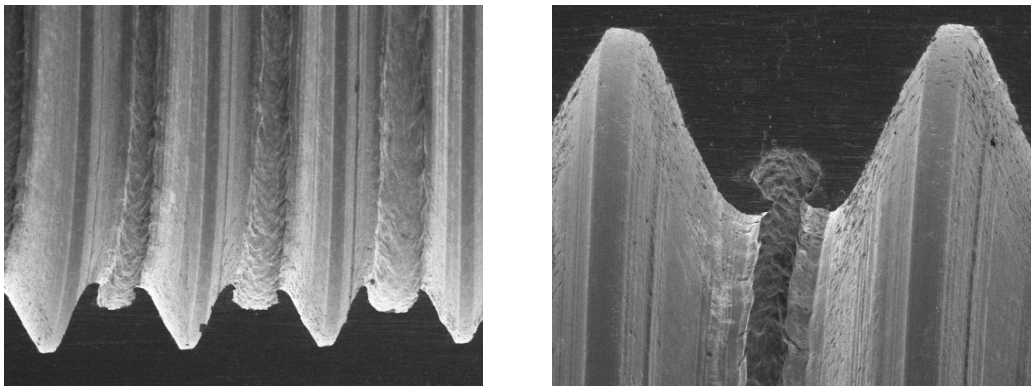

Figure 5. Microscopic morphology of the extruded thread

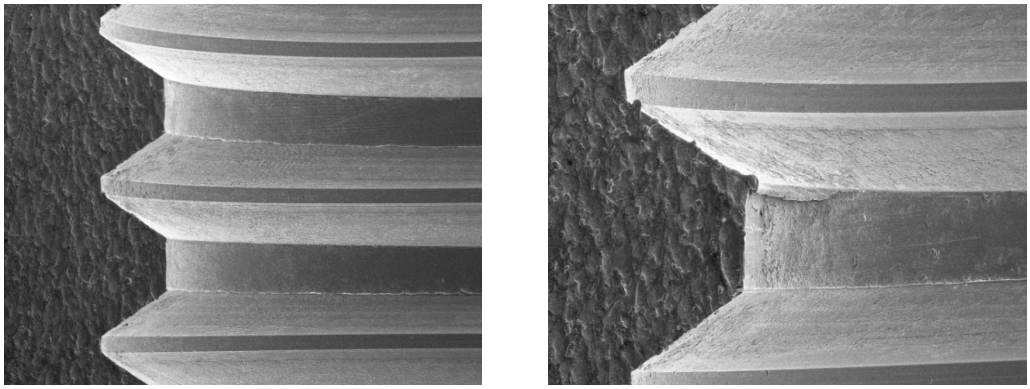

Figure 6. Microscopic morphology of the cut thread

3.2. Vickers hardness test results

The indentation positions are at the thread root and from the pitch diameter to the core. The test point locations are shown in the figure above. Five points were taken at the thread root and five points from the pitch diameter to the core for testing. The schematic diagram of the indentations is shown in Figure 7.

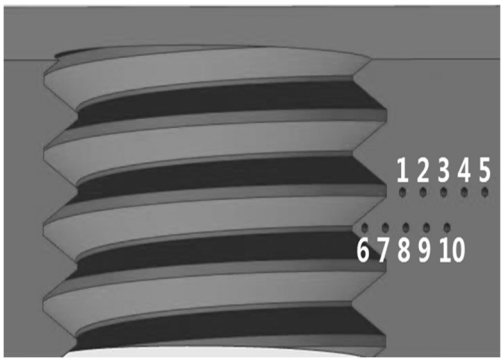

Figure 7. Schematic diagram of Vickers hardness indentation points

Internal threads are generally machined by first drilling a pilot hole and then forming the thread. For machining small-diameter internal threads, the main methods currently are thread milling and cold extrusion using a tap. Thread milling generally uses a thread milling cutter rotating at high speed to generate the minor diameter, pitch diameter, and major diameter through circular motion, and the pitch is produced through axial motion. Cold extrusion of internal threads is a chipless thread forming process. Its principle is to insert an extrusion tap into the workpiece pilot hole at a certain speed. The extrusion lobes on the tap gradually press against the inner wall of the pilot hole. As the tap continues to advance, the metal around the pilot hole flows along the surfaces of the extrusion lobes, gradually accumulates in the thread grooves, and finally forms the internal thread profile.

The Vickers hardness data at the crest and root are shown in Figure 8 and Figure 9. It can be seen that the hardness at the thread root is the highest, reaching 495 HV, and the depth of the hardened layer is between 330–350 μm. For the cut internal thread, because the metal structure is cut off and the internal structure remains almost unchanged, the hardness gradient is nearly a straight line, with an average hardness value of 416 HV. In contrast, cold extruded internal threads are formed by a plastic deformation process. The essence of metal plastic deformation is the redistribution of metal volume. After cold extrusion, not only is the metal structure not cut, but the grains are also broken, refined, and elongated. As plastic deformation progresses, the deformation resistance increases rapidly, hardness and strength also increase, while plasticity and toughness decrease, resulting in work hardening.

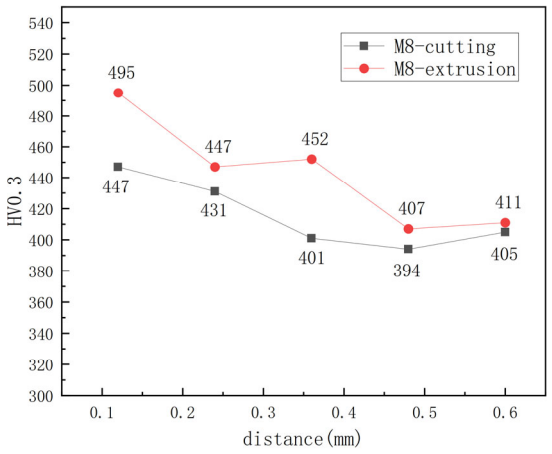

Figure 8. Vickers hardness at the thread root

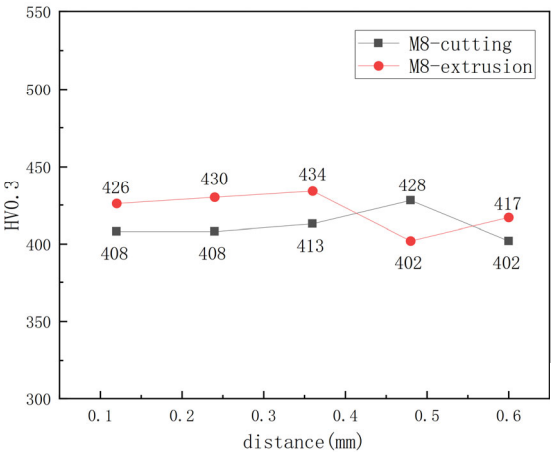

Figure 9. Pitch-to-core Vickers hardness

3.3. Mechanical property analysis

For the extruded thread, the grain boundaries of the surface metal begin to become blurred, and plastic deformation of the grains forms a strain layer. For the cut thread, no significant change is observed in the internal structure. The tensile test data are shown in Table 2. The first thread at the upper end of the extruded threaded hole has an incomplete structure, with missing thread profile in the upper half, and no complete hardened layer is formed. Subsequently, the cold extrusion process needs to be improved to avoid incomplete thread profiles and to increase extrusion strengthening at the chamfer. See Figure 10 and Figure 11.

Table 2. Tensile test data

process specifications	Specimen No.	Force at specified plastic extension/KN	average	maximum force/KN	average	Elongation after fracture A(%)
cutting machining	1#	705.7	687.5	773.0	758.8	14.5
	2#	695.1		761.8		14.0
	3#	661.6		741.6		15.5
extrusion processing	4#	680.7	696.5	754.2	765.3	14.5
	5#	716.9		777.3		14.0
	6#	691.9		764.5		14.0

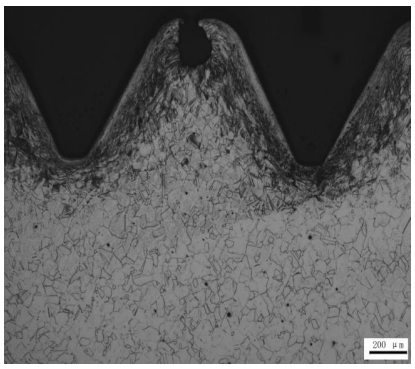

Figure 10. Microscopic morphology of the extruded thread

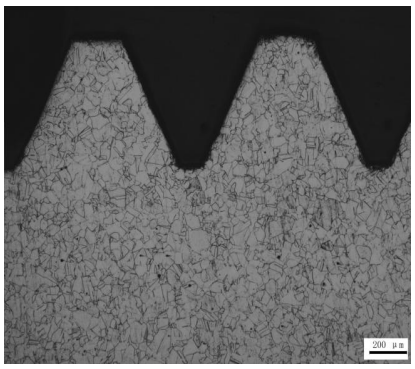

Figure 11. Microscopic morphology of the cut thread

3.4. Three-point bending fatigue test of the simulated drill collar specimen

Table 3 presents the full-scale bending fatigue test data. Under low and medium stress conditions (-4.5kN to -40kN), both types of threaded holes exhibited excellent fatigue resistance, withstanding hundreds of thousands of loading cycles without failure. The critical performance differences under high stress (-60kN) represent the load level that best distinguishes the two processing techniques. Under this high stress, the tests were no longer observed at fixed intervals but were run continuously until specimen failure. The cut specimen fractured after 24,847 cycles, while the extruded specimen fractured after 102,090 cycles. In the ultimate fatigue test leading to final fracture, the fatigue life of the extruded thread was more than four times that of the cut thread. This is a very significant performance improvement.

Under all test conditions, the threaded holes manufactured by the extrusion process showed no disadvantages. In the critical high-stress (-60kN) fatigue test that simulates extreme operating conditions, its life far exceeded that of the cut thread process.

Table 3. Full-scale bending fatigue test data

number	test force/KN	Frequency/Hz	cycles	Time/h	experimental results
cutting	-4.5	30	648000	6	no obvious cracks
	-9	30	432000	4	no obvious cracks
	-12	30	432000	4	no obvious cracks
	-40	20	432000	6	no obvious cracks
	-60	10	216000	6	no obvious cracks
	-60	10	24847	0.69	specimen fracture
extrusion	-4.5	30	648000	6	no obvious cracks
	-9	30	432000	4	no obvious cracks
	-12	30	432000	4	no obvious cracks
	-40	20	432000	6	no obvious cracks
	-60	10	72000	4	no obvious cracks
	-60	10	102090	0.84	specimen fracture

Every two hours, the test was stopped, the specimen was disassembled, and the thread was inspected for cracks. The bolt preload was 30 Nm.

3.5. Principle of fatigue fracture

Using a typical model in fracture mechanics and materials mechanics for describing the crack growth rate of metal fatigue, this model is a calculation method proposed by Paul C. Paris and F. Erdogan in 1963 for predicting the fatigue life of engineering structures[6]. The theoretical formula is as follows:

$$\frac{da}{dN} = C(\Delta k)^m \tag{3-1}$$

In the formula:

$\frac{da}{dN}$ is the crack extension per loading cycle; Δk is the stress intensity factor range($MPa \cdot \sqrt{m}$);C、 m is the material constant, where m typically ranges from 2 to 4.

$$\Delta k = Y\Delta\sigma\sqrt{\pi a} \tag{3-2}$$

In the formula:

Y is the geometric correction factor; Δσ is the stress range, MPa; a is the crack length, mm.

The non-magnetic drill collar test specimen undergoes fatigue fracture under alternating loads. Its fracture cross-section generally exhibits typical features such as the fatigue source zone, fatigue core zone, selective propagation zone, accelerated propagation zone, and instantaneous fracture zone, as shown in Figure 12-Figure 15. In Figure 13 and Figure 15, the fatigue source zone is the initiation region of the fatigue crack, mainly influenced by cyclic stress. The fatigue core zone, adjacent to the fatigue source zone, is the main region where the crack propagates slowly and stably, and it is also the core region for predicting material life. The fatigue striations in Figure 12 and Figure 14 indicate the selective

propagation zone, which may develop into fatigue damage; fatigue striations are the most typical and direct characteristic of the fatigue crack propagation zone. The accelerated propagation zone is the transition region between the stable propagation zone and the instantaneous fracture zone, where the crack length increases significantly. The instantaneous fracture zone is the final fracture part of the cross-section; after the crack reaches a critical size, unstable propagation occurs, the load exceeds the remaining load-bearing capacity of the material, and the material fractures.

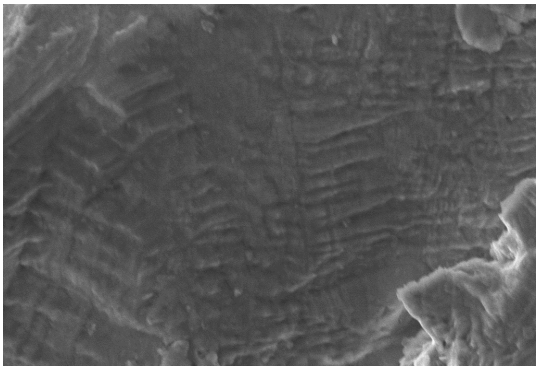

Figure 12. Fatigue striations of the extruded thread

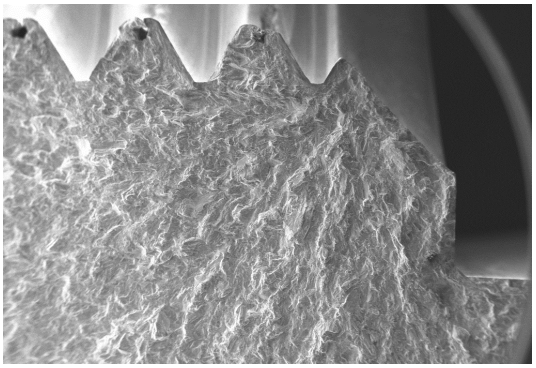

Figure 13. Fatigue source of the extruded thread

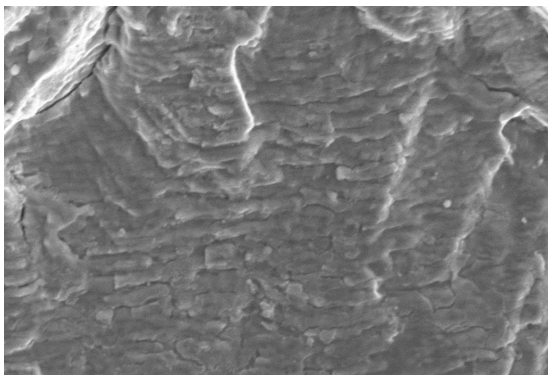

Figure 14. Fatigue striations of the cut thread

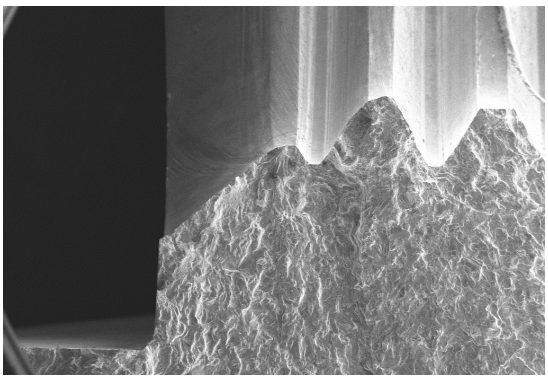

Figure 15. Fatigue source of the cut thread

4. Fatigue Calculation Results

4.1. Bending stress calculation

Formula for maximum bending stress (three-point bending):

$$\sigma_{max} = \frac{3FL}{2bh^2} \quad (4\text{-}1)$$

In the formula:

F: Test force (absolute value,N); L: span (mm); b: specimen width (mm); h: specimen height (mm).

Calculation constant: $\sigma_{max}(MPa) = F(KN) \times 12.8$

The stress ratio of this test is R = 0.1, then:

Minimum stress: $\sigma_{min} = 0.1\sigma_{max}$,Stress amplitude: $\sigma_a = (\sigma_{max} - \sigma_{min})/2$,Mean stress: $\sigma_m = (\sigma_{max} + \sigma_{min})/2$.

The calculated maximum bending stresses under various test conditions are shown in the Table 4.

Table 4. Calculated maximum bending stresses under various conditions

process	F(KN)	σ_{max}(MPa)	σ_{min}(MPa)	σ_m(MPa)	σ_a(MPa)	cycles	result
cutting	4.50	57.60	5.76	31.68	25.92	648000	unbroken
	9.00	115.20	11.52	63.36	51.84	432000	unbroken
	12.00	153.60	15.36	84.48	69.12	432000	unbroken
	40.00	512.00	51.20	281.60	230.40	432000	unbroken
	60.00	768.00	76.80	422.40	345.60	216000	unbroken
	60.00	768.00	76.80	422.40	345.60	24847	fracture
extrusion	4.50	57.60	5.76	31.68	25.92	648000	unbroken
	9.00	115.20	11.52	63.36	51.84	432000	unbroken
	12.00	153.60	15.36	84.48	69.12	432000	unbroken
	40.00	512.00	51.20	281.60	230.40	432000	unbroken
	60.00	768.00	76.80	422.40	345.60	72000	unbroken
	60.00	768.00	76.80	422.40	345.60	102090	fracture

4.2. Fatigue limit calculation

The fatigue limit is defined as the stress amplitude corresponding to 10^6 cycles (a common engineering standard):

Cutting process: σ_a >230.4MPa (the minimum stress amplitude at which the specimen did not fracture after 10^6 cycles);

Extrusion process: σ_a >230.4MPa (the minimum stress amplitude at which the specimen did not fracture after 10^6 cycles).

The data should follow the Basquin criterion (used to describe high-cycle fatigue, i.e., fatigue behavior under low strain and high cycle numbers. It assumes a power-law relationship between the fatigue life N_f and the stress amplitude σ_a):

$$\sigma_a = \sigma_f^{'}(2N_f)^b \tag{4-2}$$

In the formula:

σ_a: cyclic stress amplitude (MPa);σ'f: fatigue strength coefficient (MPa);N_f: fatigue life (cycles);b: fatigue strength exponent (usually negative).

(1) cutting process:

Substitute the data: $\sigma_a = 345.6MPa, N_f = 24847$; $\sigma_a = 230.4MPa, N_f = 10^6$,

Thus: $b = -0.1097, \sigma_f^{'} = 1132.6MPa$

Then 10^6 cycles corresponds to:

$$\sigma_a(10^6) = 1132.6 \times (2 \times 10^6)^{-0.1097} = 230.6MPa$$

(2) extrusion process:

Substitute the data: $\sigma_a = 345.6MPa, N_f = 102090$; $\sigma_a = 230.4MPa, N_f = 10^6$,

Thus: $b = -0.1777, \sigma_f^{'} = 3033MPa$

Then 10^6 cycles corresponds to:

$$\sigma_a(10^6) = 3033 \times (2 \times 10^6)^{-0.1777} = 230.24MPa$$

The cyclic stress amplitude $\sigma_a(10^6)$ at 10^6 cycles is obtained by fitting the Basquin equation. For the cutting process, it is 230.6MPa; for the extrusion process, it is 230.24MPa.

At σ_a = 345.6MPa:

Cutting process: median life ≈ 24847 cycles; Extrusion process: median life ≈ 102090 cycles. The life of the extrusion process is 4.1 times that of the cutting process.

4.3. Estimation of fatigue strength reduction factor

The fatigue strength reduction factor is a dimensionless coefficient used to describe the degree of reduction in fatigue strength of a material under cyclic loading due to factors such as surface defects, size effects, and stress concentration. It is typically used to quantify the relationship between the theoretical fatigue limit and the actual fatigue limit[7]. In this study, the influence of stress concentration at the threaded hole and the cover plate groove is considered as follows:

(1) Calculation of the theoretical stress concentration factor K_t:

For a rectangular cross-section (b = 30mm, h = 25mm) of the three-point bending specimen, with two M8×1.25 threaded holes in the center, it can be calculated as follows:

$$I = \frac{bh^3}{12} \tag{4-3}$$

In the formula:

I: moment of inertia about the neutral axis (mm4);b: specimen width (mm);h: specimen height (mm).

Then: I = 39062.5mm^4

$$W = \frac{I}{\frac{h}{2}} \tag{4-4}$$

In the formula:

W: section modulus (mm^3).

Then: W=3125mm^3.

(2) Maximum stress without hole:

$$\sigma_0 = \frac{M}{W} = \frac{\frac{F \cdot L}{4}}{W} \tag{4-5}$$

In the formula:

σ_0: maximum stress without hole (MPa);F: maximum applied load in the test (kN);L: specimen span (mm)

The maximum applied load in the test is 60kN, and the specimen span is 160mm.Substituting into the calculation yields:σ_0= 768 MPa.

(3) When a hole is present, considering stress concentration:

Under transverse bending conditions, for a strip containing two circular holes of equal diameter, when the diameter-to-width ratio d/b =0.225, the recommended value of the stress concentration factor K_t is 2.4, based on a synthesis of existing literature data and theoretical derivation.

(4) Through calculation, the actual local maximum stress is obtained as:

$$\sigma_{\max local} = K_t \cdot \sigma_0 = 2.4 \times 768 = 1843.2MPa$$

5. Comprehensive Evaluation of Fatigue Performance

5.1. Predicted life under S-N curve parameters

(1) Cutting process:

From equation (3-4) substituting the data, it can be seen that the S-N equation is: $\sigma_a = 1132.6 \times (2N_f)^{-0.1097}$

At σ_a = 345.6MPa, $N_f \approx$ 24945 cycles is calculated.

(2) Extrusion process:

From equation (3-4) substituting the data, it can be seen that the S-N equation is: $\sigma_a = 3033 \times (2N_f)^{-0.1777}$

At σ_a = 345.6MPa, $N_f \approx$ 101450 cycles is calculated.

5.2. Calculation of fatigue life scatter band

(1) Cutting process:

At σ_a = 345.6MPa, one specimen fractured at 24847 cycles, while another specimen did not fracture at 216000 cycles

(assuming it would have fractured exactly when the test was stopped). The scatter factor = 216000 / 24847 ≈ 8.69.

(2) Extrusion process:

At σ_a = 345.6MPa, one specimen fractured at 102090 cycles, while another specimen did not fracture at 72000 cycles (assuming it would have fractured exactly when the test was stopped). The scatter factor = 102090 / 72000 ≈ 1.42.

Thus, it can be seen that the life scatter of the extrusion process is smaller than that of the cutting process. Small fatigue life scatter is a comprehensive reflection of high material quality, a stable manufacturing process, and a safe and economical structural design.

6. Design and Application Recommendations

6.1. Theoretical predicted value

In the fitted S-N equation, calculate the theoretically predicted stress amplitude for the case where $N_f = 10^5$ (which is a typical representative of high-cycle fatigue).

(1) cutting process:

$$\sigma_a = 1132.6 \times (2N_f)^{-0.1097}$$

substitute $N_f = 10^5$, we get: $\sigma_a \approx 296.9MPa$.

(2) extrusion process:

$$\sigma_a = 3033 \times (2N_f)^{-0.1777}$$

substitute $N_f = 10^5$, we get: $\sigma_a \approx 346.6MPa$.

6.2. Determination of safety factor

Due to the scatter in fatigue tests, a safety factor n needs to be introduced. Based on the previous scatter band factors and the required range, according to the test data, the scatter of the cutting process (scatter band factor approximately 8.69) is larger, so n = 1.1 is taken; the scatter of the extrusion process (scatter band factor approximately 1.42) is smaller, so n = 1.15 is taken.

Calculate the allowable stress amplitude:

$$[\sigma_a] = \frac{\sigma_a}{n} \tag{6-1}$$

In the formula:

$[\sigma_a]$: allowable stress amplitude (MPa)

Substituting the predicted value and the safety factor, we obtain:

$$[\sigma_a]_{切削} \approx 270MPa \qquad [\sigma_a]_{挤压} \approx 301.4MPa$$

If the actual working stress amplitude is 345.6MPa, then the corresponding safety factor is:

$$n_{切削} = \frac{345.6}{270} \approx 1.28 \qquad n_{挤压} = \frac{345.6}{301.4} \approx 1.15$$

7. Conclusion

(1) The cracks in the threaded holes of the non-magnetic drill collar formed by cutting are high-cycle fatigue cracks generated during service. The initiation and propagation of fatigue cracks are due to the combined effect of rotating bending stress and vibration stress.

(2) Under all test conditions, the threaded holes manufactured by the extrusion forming process showed no disadvantages. In the critical high-stress (-60kN) fatigue test that simulates extreme operating conditions, its life far exceeded that of the cutting forming process. Cold extrusion utilizes the plastic deformation characteristics of materials at low temperatures. During the deformation process, the crystal structure inside the metal changes, typically resulting in a cold work hardening effect, thereby increasing the strength and hardness of the material.

(3) The fatigue limit lives under the two different processes were estimated, and the data should follow the Basquin criterion. After fitting, the median lives at a stress amplitude σa = 345.6MPa under 10^6 cycles were obtained: approximately 24847 cycles for the cutting process and approximately 102090 cycles for the extrusion process. In the ultimate fatigue test leading to final fracture, the fatigue life of the extruded thread was more than four times that of the cut thread. This is a very significant performance improvement. Threads treated by cold extrusion generally have higher fatigue strength, can withstand higher cyclic loads, and have a longer service life.

(4) The influence of stress concentration at the threaded hole and the cover plate groove should be considered. After incorporating the stress concentration factor Kt, the actual local maximum stress is calculated to be 1843.2MPa. This may cause the thread root or the sharp corner of the cover plate groove to be the origin point of fatigue cracks, which is consistent with the observation in the test that cracks occurred at the threads.

(5) At σ_a = 345.6MPa, the scatter band factor of the cutting process is 8.69, and that of the extrusion process is 1.42. Thus, it can be seen that the life scatter of the extrusion process is smaller than that of the cutting process. Small fatigue life scatter is a comprehensive reflection of high material quality, a stable manufacturing process, and a safe and economical structural design.

(6) Differentiated determination of safety factors based on the characteristics of the test data. In view of the inherent data scatter in fatigue tests and the difference in scatter band factors between the two processes, the safety factors are determined differentially: for the cutting process, the scatter band factor is approximately 8.69, indicating greater data scatter, so a safety factor of n=1.1 is adopted; for the extrusion process, the scatter band factor is approximately 1.42, indicating smaller data scatter, so a safety factor of n=1.15 is adopted. This approach balances the safety and rationality of the allowable stress values.

References

[1] Wu J X.Study on hot deformation behavior of high nitrogen austenitic stainless steel for non-magnetic drill collar[D]. Northeastern University,2020.

[2] Zhang Y L, Guo C, Shang J, et al. Fracture failure analysis of drill collar for logging while drilling tool[J].China Metallurgy, 2022, 32(9), 37-44.

[3] Wang J C, Zhao H Y, Jiang T, et al. Hot deformation behavior of P550 steel for non-magnetic drill collar[J].Journal of Plasticity Engineering, 2024, 31(11), 167-176.

[4] Qin C H, Wang Y Y, Xu Z G, et al. Microstructure and fatigue life of P550 non-magnetic drill collar threaded holes under different forming processes[J].Journal of Precision Forming Engineering, 2025, 17(4), 160-169.

[5] Chen X .Research on forming process and quality of internal thread by cold extrusion[D]. Shaanxi University of Technology, 2022.

[6] Chen L, Huang T L, Zhou H. Stochastic model of metal fatigue crack growth based on proportional Paris formula and inverse Gaussian process[J].Engineering Mechanics, 2021, 38(10), 238-247.

[7] Zhao S B.Anti-fatigue Design Manual[M]. China Machine Press, 2015.